Prior Signal Acquisition Software Versions for Orbitrap Underestimate Low Isobaric Mass Tag Intensities, Without Detriment to Differential Abundance Experiments

Tom S Smith*, Anna Andrejeva, Josie A. Christopher, Oliver M. Crook, Mohamed A. W. Elzek, Kathryn S Lilley

* Corresponding author. Email: tss38@cam.ac.uk

1   **Abstract**

2

3   Tandem mass tags (TMT) enable simple and accurate quantitative proteomics for
4   multiplexed samples by relative quantification of tag reporter ions. Orbitrap™
5   quantification of reporter ions has been associated with a characteristic notch region in
6   intensity distribution, within which few reporter intensities are recorded. This has been
7   resolved in version 3 of the instrument acquisition software, Tune. However, 53 % of
8   Orbitrap Fusion, Lumos or Eclipse submissions to PRIDE were generated using prior
9   software versions. To quantify the impact of the notch on existing quantitative
10   proteomics data, we generated a mixed species benchmark and acquired quantitative
11   data using Tune versions 2 and 3. Sub-notch intensities are systemically
12   underestimated with Tune version 2, leading to over-estimation of the true differences in
13   intensities between samples. However, when summarising reporter ion intensities to
14   higher level features, such as peptides and proteins, few features are significantly
15   affected. Targeted removal of spectra with reporter ion intensities below the notch is not
16   beneficial for differential peptide or protein testing. Overall, we find the systematic
17   quantification bias associated with the notch is not detrimental for a typical proteomics
18   experiment.

Introduction

Bottom-up quantitative proteomics entails proteolytic digestion of proteins to peptides, quantification of peptide abundances by mass spectrometry (MS) and summarisation of protein abundances. Data-dependent acquisition (DDA) is the classical acquisition mode. Due to the stochastic nature of peptide selection, not all peptides present in a sample are fragmented and sequenced, with data completeness diminishing as the number of samples increases [1]. Missing values are reduced with data-independent acquisition (DIA) approaches [2], although there are still detection threshold limits and samples cannot be multiplexed in typical DIA workflows.

Alternatively, samples may be labelled with isobaric tags which possess the same mass, but different distributions of heavy isotopes within the tags, such that a sample-specific mass reporter tag is released by high energy collision-induced dissociation [3]. By enabling sample multiplexing, the frequency of missing values is thus reduced compared to Label Free Quantification [4]. Furthermore, all samples are quantified from the same peptide spectrum matched (PSM) ions, greatly simplifying summarisation to protein-level abundances [5].

Tandem Mass Tags (TMT) are the most commonly used isobaric tags, with current chemistry allowing up to 18 samples to be multiplexed [6]. Since quantification is typically of the tag rather than the peptide, TMT proteomics has been shown to suffer ratio compression by the presence of co-isolated 'interference' peptides [7]. Such compression can be partially mitigated by use of synchronous precursor selection (SPS)-MS3 quantification [8]. Thus, robust quantification of TMT labelled peptides requires high-resolution, accurate mass spectrometers, with Orbitrap™ devices being commonly employed. Intriguingly, a recent characterisation of TMT reporter ion signals obtained from Orbitrap identified a consistent absence of intensities within a specific range, which visually appears as 'notch' in the distribution of intensities [9]. The presence of the notch was determined to depend on the automatic gain control (AGC) target and maximum injection time Orbitrap parameters, with higher values reducing its prominence. Hughes *et al* hypothesised the cause of the notch is rooted in the signal processing behaviour, from their observation of a notch in all datasets acquired via Orbitrap-based measurements, regardless of the other associated MS hardware, and the exhaustive consideration of user-defined parameters. Hughes *et al* further speculated that standard procedures to remove low-intensity spectra would mitigate any potential issues with quantification inaccuracies.

The release notes for the Orbitrap Fusion Series 3.0 signal acquisition software, Tune, explain that the notch has been resolved in Item DE 54684: 'Addressed the peak

59   intensity (linearity) for extremely low S/N values' [10]. Nevertheless, published datasets

60   have used prior software versions and trust in the results from these experiments is

61   contingent upon accurate quantification.

62

63   Here, we further examine the 'notch' phenomenon and demonstrate what happens to

64   reporter ion intensities that fall inside the notch. Crucially, we examine the overall

65   impact of the notch for the detection of significant fold changes and estimation of their

66   magnitude, in an experiment that aims to measure differential abundance.

67

68   **Results and discussion**

69

70   To estimate the proportion of published Orbitrap datasets using Tune versions that will

71   generate a notch, we downloaded .raw files from PRIDE for all studies using only

72   Orbitrap Fusion, Lumos or Eclipse hardware since these use the same series of

73   acquisition software. We then extracted the version of Tune used from the .raw file (see

74   methods). In total, 1283 studies were examined, with the remaining studies either

75   falsely stating the instrument model, or not possessing files that could be parsed for

76   meta data (Figure 1a). Overall, 53.0 % of studies used Tune versions that generate a

77   notch, including 27.3 % of submissions in the year to 28th June 2021. It is therefore

78   imperative to determine what impact the notch has on quantitative proteomics.

79

80   We first reanalysed previously published Orbitrap SPS-MS3 TMT data acquired using

81   Tune v2 to demonstrate that average signal/noise filtering is not a sufficient remedy for

82   the notch. Between 3.9-4.5 % tag intensities fell within or below the notch (Figure 1b &

83   S1b-c) in our U-2 OS LOPIT-DC [11] experiments, with the proportion varying

84   considerably between tags within a given experiment (Figure S1d-f). Using increasingly

85   stringent filtering to remove PSMs with low average signal/noise ratios reduces the

86   proportion of sub-notch values (Figure 1c-d). However, even after removing PSMs with

87   average signal/noise less than 100, 0.24-0.69 % of remaining tag intensities are below

88   the notch, whilst 52.8-55.0 % of quantified PSMs are discarded. Using a more moderate

89   10-fold filter, as previously suggested [12], removes 6.6-6.8 % of the quantified PSMs,

90   with 1.2-1.8 % of the remaining reporter intensities being below the notch. Thus, while

91   average signal/noise filtering will increase quantification accuracy, it is not a complete

92   remedy for sub-notch values.

93

94   To demonstrate what happens to notch intensities, we used redundant PSMs to predict

95   expected reporter ion intensities. In brief, we considered sets of PSMs from the same

96   peptide sequence and used the reporter ion intensities from the highest intensity PSM

97   to predict the expected reporter ion intensity values for the other PSMs (see methods).

98   Predicted and observed tag intensities were highly correlated, confirming the validity of

99   this approach (Figure 1e, S2a-b). As expected, intensities below the notch are
100   systematically under-estimated relative to the prediction (Figure 1f, S2c-d).
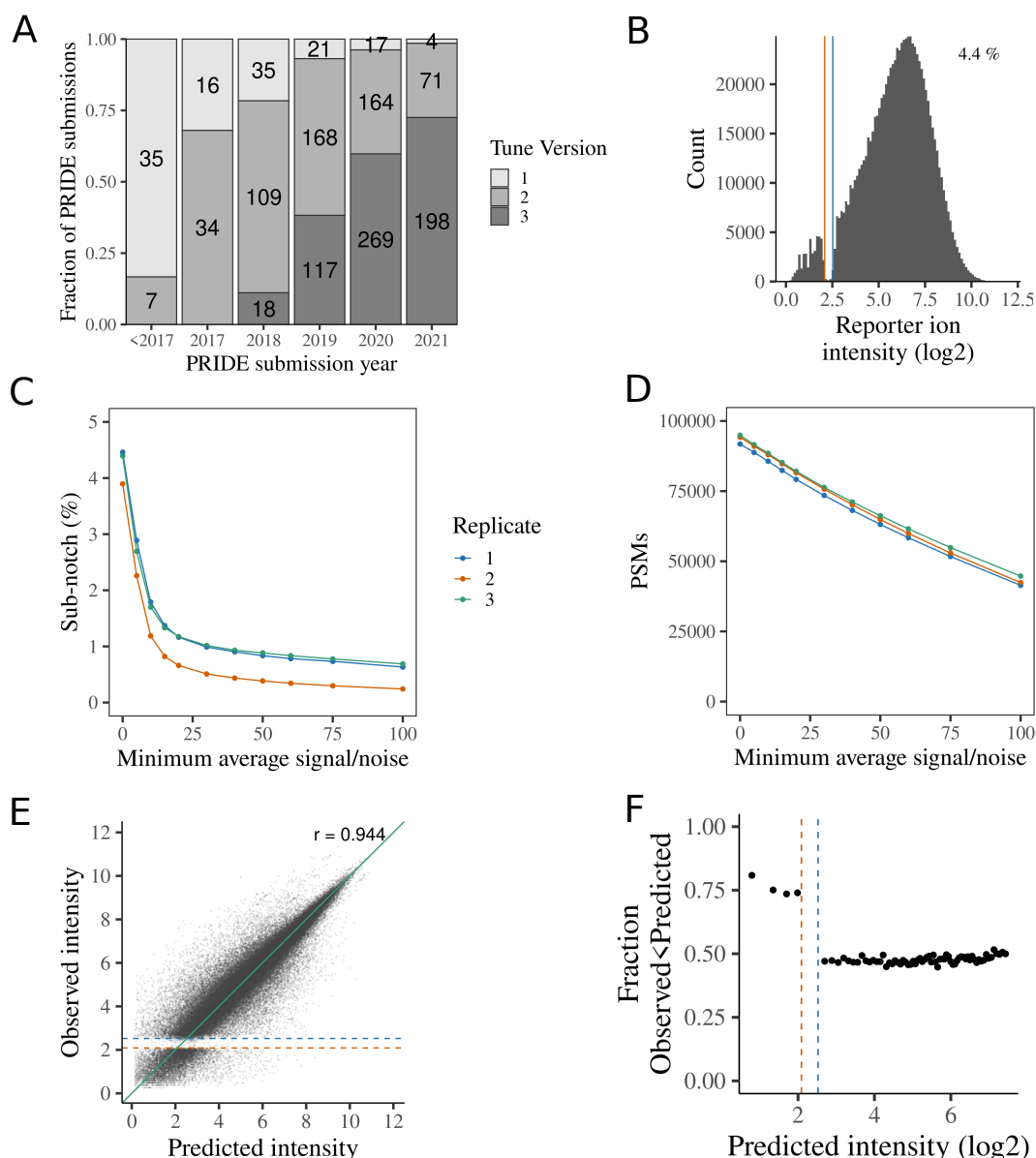101

102
103   Figure 1. (A) Tune major versions for Orbitrap Lumos, Fusion and Eclipse PRIDE submissions (B) The
104   distribution of ion signals for TMT reporters U-2 OS LOPIT-DC, replicate 1. The percentage of tag
105   intensities below the upper boundary of the notch is stated in the top right corner. (C-D) The impact of
106   filtering PSMs by their average signal/noise. (C) The proportion of reporter tag intensities at or below the
107   notch. (D) The number of PSMs remaining. (E) Observed tag intensities vs predicted tag intensities.
108   Green line is equality. Pearson product-moment correlation coefficient shown in the top right corner (F)
109   Fraction of observed tag intensities that are below the prediction for binned predicted tag intensity.
110   Observed tag intensities below the notch are systematically underestimated relative to the prediction. The
111   approximate boundaries of the notch region are denoted by vertical or horizontal lines in B, E and F.
112   Equivalent plots for replicate 2 and 3 are shown in Figure S1-2.

113

114   To explore the impact of the notch and sub-notch region on a typical quantitative TMT
115   MS3 proteomics experiment, we considered suitable published benchmark experiments.
116   Hughes *et al* performed a spike-in benchmark experiment to assess the impact of the
117   notch [9]. However, this included only 550 spike-in peptides, precluding a consideration of
118   the impact of the notch in a routine proteomics experiment. In another benchmarking
119   study, O'Connell *et al* spiked peptides from *S.cerevisiae* cell lysates into *H.sapiens*
120   peptide samples at known concentration, thus mimicking a control vs treatment(s)
121   differential protein abundance experimental design [4]. However, the authors used a
122   relatively high AGC target of 20,000 and maximum injection time of 150 ms. Thus, only
123   0.6 % tag intensities were observed at or below the notch, preventing any analysis of
124   the impact of the notch in a more typical setting (Figure S3a). We therefore created our
125   own spike-in benchmark experiment, aiming to observe a notch with typical prominence
126   (see methods). Proteins extracted from whole cell lysates of *S.cerevisiae* and *H.sapiens*
127   osteosarcoma cell line U-2 OS were digested to peptides and mixed, such that
128   *S.cerevisiae* peptides were at 1x (5µg), 2x and 6x volumes in a total of 100 µg peptide.
129   Thus, we generated differences in protein abundance between 1.06 - 6-fold for
130   *H.sapiens* and *S.cerevisiae* proteins. Peptides were then labeled with TMT and
131   quantified on an Orbitrap Mass Spectrometer with Tune 2.1 and Tune 3.4, with an AGC
132   target of 50,000 and max injection time of 120 ms, which we expected to yield a
133   moderate and typical notch [9] (see methods for details). Using these parameters and
134   Tune 2.1, 3.2 % of tag intensities were within or below the notch (Figure 2b), with
135   *S.cerevisiae* peptides showing a slightly greater proportion of low tag intensities (Figure
136   S3b-c). In total we obtained 109,779 PSMs from 10,982 protein groups, of which 8,335
137   and 2,469 could be assigned to *H.sapiens and S. cerevisiae*, respectively.

138

139   We applied strict filtering to minimise the possibility of PSM mis-identification or
140   interference, demanding co-isolation < 10 %, and delta score > 0.5, with the later
141   ensuring that rank 2 peptide matches for a given spectrum have a score less than half
142   the rank 1 peptide match. We further removed PSMs with average reporter signal/noise
143   < 10. Using these thresholds, 19,975 PSMs were retained. As expected, sub-notch tag
144   intensities were clearly underestimated, with the correct fold-change only observed
145   when reporter ion intensities were above the notch (Figure 2c). In contrast, using Tune
146   3.4, no notch was visible (Figure S4a) and the underestimation of fold-changes at low
147   reporter ion intensity was largely resolved (Figure S4b).

148

149   We then aggregated reporter intensities to protein-level intensities, requiring at least two
150   PSMs per protein. The majority of protein-level quantification estimates did not involve
151   sub-notch intensities, with a maximum of 63 proteins (1.7%) having 25 % or greater
152   sub-notch ion intensities in any given tag (Figure S5a).

153

154   To formally test the impact of the notch on the detection of peptide or protein differential
155   abundance, we used *limma* to detect differential abundance, with and without prior
156   filtering to remove PSMs containing intensities at or below the notch. The accuracy for
157   identification of changes in intensity was measured by the F1 score, the harmonic mean
158   of precision and recall. Fold-change estimates were very slightly closer to ground truth
159   without notch filtering, but the difference was negligible (Figure S5b). For example,
160   median fold-changes for *S.cerevisiae* proteins in the 6x vs 1x comparison decreased
161   from 4.963 to 4.949 (Figure S6a). Crucially, notch filtering did not improve the F1 score
162   for the most difficult to identify changes (*H.sapiens* 2x vs 1x) which was 0.245 and
163   0.246, respectively, with and without notch filtering (Figure S6b). Similarly, for the easier
164   to detect fold changes, F1 was not significantly affected by notch filtering.

165

166   To ensure that our observations were not dependent on the PSM filtering, we varied the
167   thresholds for maximum interference (10%, 50%, 100%), minimum average signal/noise
168   (0, 10) and minimum Delta score (0, 0.2, 0.5). Each combination of PSM filtering
169   thresholds was repeated with and without removing PSMs with sub-notch values. Thus,
170   in total, 36 PSM filtering regimes were compared, representing a comprehensive set of
171   PSM filtering schemas. Regardless of the thresholds used, notch filtering had negligible
172   impact on fold-change estimates or the F1 score, whilst always reducing the number of
173   proteins that could be interrogated (Figure S6). Thus, removing PSMs with sub-notch
174   values does not appear to be beneficial and may even reduce sensitivity in differential
175   protein abundance experiments.

176

177   Finally, we repeated the differential abundance testing at the peptide-level. Whilst
178   differential abundance testing is more typically performed at the protein level, there are
179   experiments where peptide-level testing is more appropriate, including in the analysis of
180   post-translational modifications[12]. Given fewer reporter ion intensities are used to
181   quantify peptides, we expected a more significant impact from the removal of sub-notch
182   intensities. However, no improvements in the fold-changes were observed (Figure S5c)
183   and the increase in F1 score was typically 0.001-0.005 and thus too slight to justify
184   notch filtering (Figure S7).

185

186   To inspect the impact of the notch filtering on the estimated fold changes more directly,
187   we considered proteins where at least one PSM was removed in the filtering, and
188   compared the fold changes with and without notch filtering. As previously described, the
189   proportion of proteins with a sub-notch PSM is relatively low. When using stringent PSM
190   filtering, just 120 protein fold-changes are affected by the sub-notch filtering, of which
191   116 are yeast proteins. The clear majority of fold-changes are further from the ground
192   truth when notch filtering is used (Figure 2d). This observation is counter-intuitive given
193   that sub-notch values are systematically underestimated, suggesting their removal

194   should yield more accurate fold-change estimates. However, since TMT fold-change
195   estimates are always compressed to some extent [5,7], the underestimation of these very
196   low intensities below the notch can act to counter the ratio compression. Whilst this is
197   not a justification for retaining the notch to improve fold-change estimates, it further
198   underlines the negligible impact the notch and sub-notch values should have on typical
199   proteomics experiments, where higher level features are typically summarisations of
200   multiple independent PSMs.

201

202   An important caveat to our observations is that our benchmark experiment possessed a
203   typical notch prominence and was designed to mimic a simple experiment to detect
204   differential protein abundance. It is possible that in datasets with a more prominent
205   notch, the underestimated tag intensities could become more problematic. Additionally,
206   the notch could conceivably be more problematic where accurate quantification of the
207   ratios between tags are more important than identifying significant differences between
208   treatment groups. For example, in thermal proteome profiling, sub-notch intensities
209   could lead to more poorly fitted curves or models in some edge cases [13]. If sub-notch
210   values were found to be detrimental in specific applications, we expect that imputing
211   sub-notch values will rectify this. Setting aside these caveats, we believe this artifact in
212   existing Orbitrap Fusion, Lumos and Eclipse quantification data using Tune < 3.0 can be
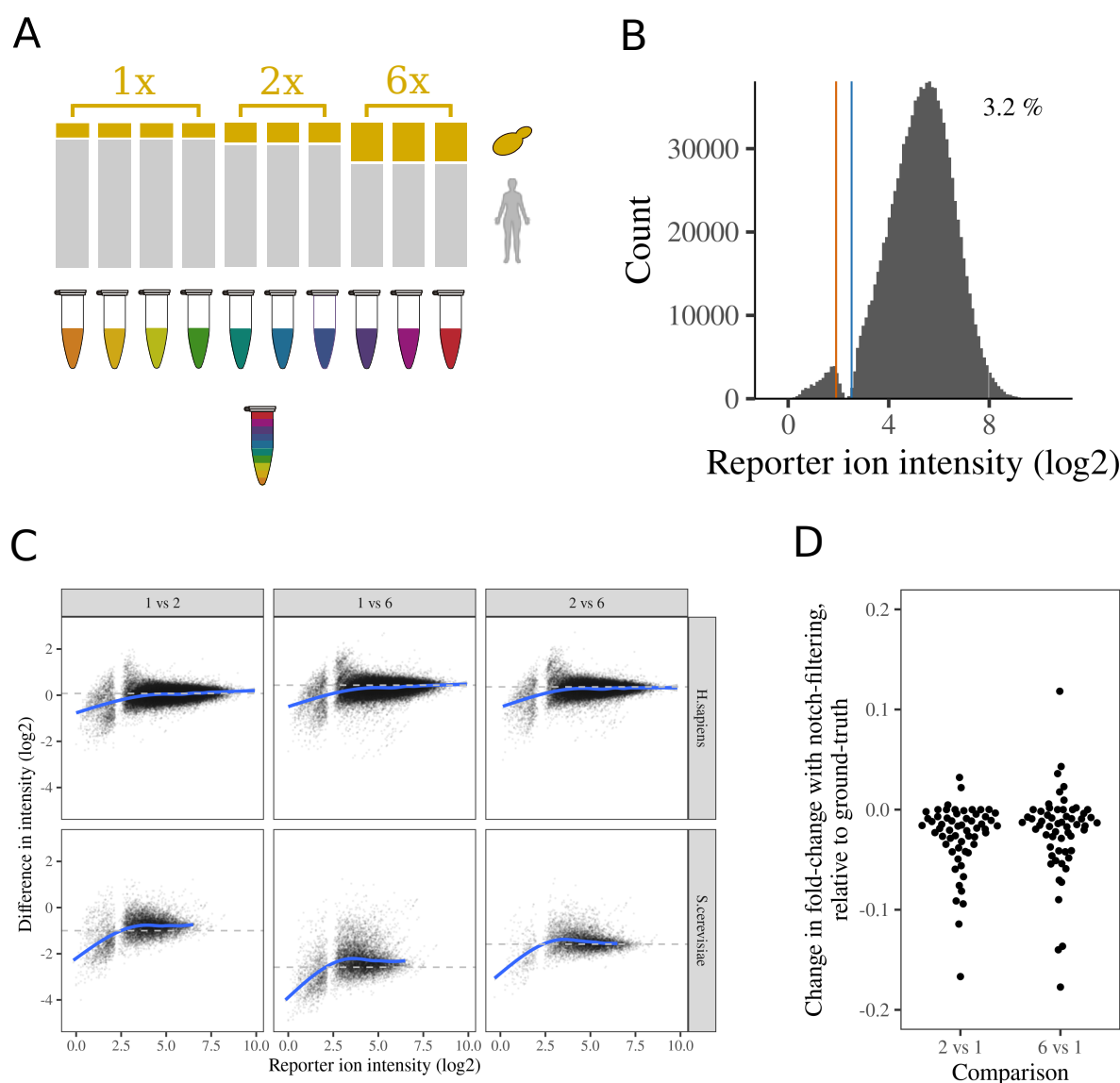213   safely ignored for routine proteomics experiments.

214

Figure 2. Impact of the notch on a differential expression benchmark proteomics experiment. (A) Schematic representation of benchmark TMT proteomics experimental design. Yeast peptides were spiked into human peptides at 1x, 2x and 6x volumes to induce ground truth fold-changes for both yeast and human proteins and labelled with TMT (B) The distribution of reporter ion intensities for TMT reporters. The approximate boundaries of the notch region are denoted by vertical lines. The percentage of tag intensities below the upper boundary of the notch is stated in the top right corner. (C) The difference between a single tag intensity and the mean tag intensity for a comparator group of tags. The ground truth is denoted by a dashed horizontal line. The blue line presents a generalized additive smoothing model for the relationship between tag intensity and intensity difference. (D) The difference in fold change when including notch filtering, relative to the ground truth. Positive values represent fold-change estimates closer to ground truth upon notch filtering. Only yeast proteins with at least one sub-notch reporter ion intensity are shown.

229 **Experimental section**
230

231 *Cell culture and harvest*

232

233 *S. cerevisiae* (EOROSCARF; BY4742 (MATα his3Δ1 leu2Δ0 lys2Δ0 ura3Δ0)) were
234 inoculated into YPD media (Bacto-peptone, yeast extract, 50% glucose) at 32°C with
235 constant agitation. Cells were collected by centrifugation when grown to an optical
236 density OD600 ~ 0.5, corresponding to exponential phase, and snap-frozen in liquid
237 nitrogen until lysis. Cell pellets were resuspended in lysis buffer (200 mM HEPES (pH
238 8.5), 8M urea, 0.2% SDS) supplemented with protease and phosphatase inhibitors
239 (Roche cOmplete mini EDTA-free protease inhibitor cocktail; 11873580001, Roche
240 PhosSTOP; 4906845001) and mechanically disrupted with glass beads (MERCK;
241 G8772) using a FastPrep-24™ 5G (MP Biomedicals SKU; 116005500) with the
242 manufacturer's pre-defined programme for yeast sample lysis (40 sec mixing at 40 m/s).
243 The lysate was centrifuged to pellet cell debris and supernatant transferred to a fresh
244 tube.

245

246 Human epithelial bone osteosarcoma, U-2 OS (ATCC® HTB-96™) cells were cultured
247 and incubated in McCoy's 5A (Gibco™; 16600082) supplemented with 10% FBS at
248 37°C in humidified conditions with 5% CO2 and tested to confirm absence of
249 Mycoplasma. Cells were harvested at ~90% confluence by scraping directly from the
250 plate in chilled lysis buffer (as used in yeast lysis) and sonicated on high setting for a
251 total of 15 minutes (30 sec cycles) at 4°C using a Bioruptor® Plus. The lysate was
252 centrifuged to pellet cell debris and supernatant transferred to a fresh tube.

253

254 *Reduction, alkylation & digestion*

255 Nuclease enzyme (Millipore Benzonase® Nuclease HC; 71206-3) was added to cell
256 lysates to breakdown interfering DNA before quantification of protein concentration by
257 BCA assay (Thermo Scientific 23225) according to manufacturer instruction. Disulphide
258 bonds in the lysates were reduced with 15 mM dithiothreitol (DTT) for 1 hr at 37°C,
259 followed by alkylation with 55 mM iodoacetamide (IAA) for 1 hr at room temperature in
260 the dark. To remove urea and other substances that could interfere with digestion,
261 lysates were precipitated using chilled 50:50 ethanol:acetone overnight at -20°C. The
262 resulting protein pellets were then resuspended in 200 mM HEPES (pH 8.5) and
263 sonicated for a total of 15 minutes (30 sec cycles) to break up the pellets. Proteins were
264 digested in a two-step digestion with 100:1 protein:protease ratio of Lys-C (Promega;
265 V1671) 37○C for 4 hr, followed by 100:1 trypsin digestion (Promega; V5111) at 37○C
266 overnight.

267

268   *Peptide mixing & TMT labelling*

269   Peptide concentrations were measured by using a fluorometric peptide assay (Pierce;
270   23290) before preparing human/yeast species mixes to specified ratios. 5 µg yeast
271   peptides were used for tags 126, 127N, 127C and 128N, 10 µg for 128C, 129N and
272   129C, and 30 µg for 130N, 130C and 131. The samples were made up to 100 µg using
273   human peptides, TMT-labelled (Thermo Scientific; 90406) according to manufacturer's
274   instructions, pooled and lyophilized.
275

276   *Peptide clean up & offline pre-fractionation*

277   The multiplexed sample was desalted using solid phase extraction (SPE) with a C18
278   cartridge (Waters SepPak®; WAT054955) by binding and washing peptides with 0.1%
279   trifluoroacetic acid (TFA) and eluting desalted peptides with 70% acetonitrile/0.05%
280   acetic acid. Peptides were separated using a basic pH reverse-phase liquid
281   chromatography (RP-LC) on a Acquity UPLC system with a diode array detector (210-
282   400 nm) to monitor elution profiles. Peptides were eluted with an Acquity UPLC BEH
283   C18 column (2.1-mm ID × 150-mm; 1.7-µm particle size) (Waters; 186002353) over a
284   50 min linear gradient from 5 to 75% acetonitrile in ammonium formate (pH 10.0) at a
285   flow rate of 0.244 mL/min. A total of 34 fractions were taken from the elution gradient
286   and concatenated into 15 fractions. Samples were subsequently dried and solubilised in
287   0.1% formic acid.

288

289   *Mass spectrometry data acquisition*

290   TMT labelled samples were analysed using a Dionex Ultimate 3000 RSLC nanoUPLC
291   (Thermo Fisher Scientific Inc, Waltham, MA, USA) system online with an Orbitrap
292   Lumos mass spectrometer (Thermo Fisher Scientific Inc, Waltham, MA, USA), data was
293   collected using both Tune 2.1 and 3.4 version Peptides were loaded onto a trap-column
294   (Thermo Scientific PepMap 100 C18, 5 µm particle size, 100A pore size, 300 µm i.d. x
295   5mm length) and separation of peptides was performed by C18 reverse-phase
296   chromatography at a flow rate of 300 nL/min and a Thermo Scientific reverse-phase
297   nano Easy-spray column (Thermo Scientific PepMap C18, 2µm particle size, 100A pore
298   size, 75µm i.d. x 50cm length). All samples were acquired in a 120 min run applying
299   data acquisition using synchronous precursor selection MS^3 (SPS-MS3) [8]. Analytical
300   chromatography consisted of Buffer A (HPLC H_2O, 0.1% formic acid) and Buffer B (80%
301   ACN, 0.1% formic acid). 0-3 min at 2% buffer B, 3-93 min linear gradient 2% to 40%
302   buffer B, 93-100 min linear gradient 40% to 90% buffer B, 100-104 min at 90% buffer B,
303   104-105 min linear gradient 90% to 2% buffer B and 105-120 min at 5% buffer B.

304   All *m/z* values of eluting peptide ions were measured in an Orbitrap mass analyzer, set
305   at a resolution of 120,000 and were scanned between *m/z* 380-1500 Da. Data
306   dependent MS/MS scans (3 second duty cycle time) were employed to automatically
307   isolate and fragment precursor ions using Collisional-Induced Dissociation (CID)
308   (Normalised Collision Energy of 35%). Only precursors with charge between 2 to 7 were
309   selected for fragmentation, with an AGC target of 10,000 and maximum accumulation
310   time of 50 ms. Precursor isolation was performed by the quadrupole with 0.7 m/z
311   transmission window. MS2 fragments were measured with the Ion Trap analyser.
312   Dynamic exclusion window was set to 70 seconds. SPS ions were all selected within
313   the 400–1,200 m/z range. AGC targets and maximum accumulation times were set to
314   50,000 and 120 ms respectively. Ten co-selected precursors for SPS-MS3 underwent
315   Higher energy Collisional-induced Dissociation (HCD) fragmentation with 65%
316   normalized collision energy and were analysed in the Orbitrap with nominal resolution of
317   50 000. Data was acquired with equivalent parameters for both version of Tune, 2.1 and
318   3.4.

319   *Mass spectrometry data analysis*

320   Raw data were viewed in Xcalibur v3.0.63 (Thermo Fisher Scientific), and data
321   processing was performed in Proteome Discovered v2.4 (Thermo Fischer Scientific).
322   Reference *Homo sapiens* and *Saccharomyces cerevisiae* fasta databases containing all
323   review UniProt/Swiss-Prot entries were downloaded from www.uniprot.org on April 2018
324   and June 2020, respectively. The raw files were submitted to a database search using
325   PD with Sequest HF algorithm using the concatenated reference databases and the
326   Common contaminant database [14]. The peptide and fragment mass tolerances were set
327   to 10 ppm and 0.5 Da, respectively. Static modification carbamidomethyl on cysteine
328   was applied as well as TMT-6plex tagging of lysines and peptide N terminus. Oxidation
329   of methionine and deamidation of asparagine and glutamine were included as variable
330   modifications and up to two missed cleavages were allowed. Percolator node was used
331   for false discovery rate estimation and only rank one peptides identifications of high
332   confidence (FDR < 1%) were accepted.

333   Previously published data [4,11] was downloaded from pride accessions PXD011254 and
334   PXD007683 in raw format. Raw data was re-analysed as indicated above, except that
335   the reference proteomes for *H.sapiens* (UP000005640) and *Saccharomyces cerevisiae*
336   (UP000002311) were downloaded in fasta format on 17 January 2020 and used for
337   database searching with Mascot server (ver. 2.4, Matrix Science)
338
339   *Data processing and analysis*
340

341 PSM-level quantification was exported from Proteome Discoverer in text format.
342 Downstream processing, analysis, aggregation and visualisation performed using R [15]
343 v4.0.3 "Bunny-Wunnies Freak Out" and the tidyverse [16], MSnbase [17] and camprotR
344 (https://github.com/CambridgeCentreForProteomics/camprotR) packages.
345
346 PSM quantifications were filtered to remove potential contaminating proteins using the
347 cRAP database [14]. Based on a visual assessment of the tag intensity distributions, the
348 approximate boundaries of the notch were denoted as 4.25 and 5.75.
349
350 For the prediction of expected reporter ion intensities with the reanalysed data, PSMs
351 with the same sequence within an experiment were grouped, excluding groups with only
352 one PSM, or where the highest intensity PSM contained missing values. Intra-group
353 intensity adjustment factors were then calculated, representing the intensities of each
354 PSM relative to the most intense PSM, using only the channels without missing values.
355 The highest intensity PSM was then normalised by dividing each tag intensity by the
356 total PSM intensity, such that the total normalised intensity was 1. These normalised
357 intensities were then multiplied by the adjustment factors to yield tag intensity
358 predictions for each PSM in the group, except the highest intensity PSM.
359
360 To explore the relationship between tag intensities in the benchmark dataset, individual
361 tag intensities were compared to the mean value for a comparator group of tags. A
362 generalized additive smoothing model for the relationship between tag intensity and
363 intensity difference was fitted using the default model for the ggplot function
364 geom_smooth with method='gam', namely the gam function in mgcv, with options
365 'formula = y ~ s(x, bs = "cs")' and 'method = "REML"'.
366
367 Prior to PSM filtering, to remedy any small difference in the total tag intensity in each
368 channel, PSM intensities were log center-median normalised, before exponentiating
369 back to the untransformed values.
370
371 PSM filtering was performed using 4 PSM metrics: (1) Delta score, which represents the
372 normalised difference in the spectrum matching scores between the top ranked and
373 second ranked peptides, calculated as delta = (rank 1 score - rank 2 score) / rank 1
374 score, and is thus bounded between 0 (no difference) and 1 (no rank 2 score). (2) Co-
375 isolation, calculated as: 100 * (1 - (precursor intensity in isolation window / total intensity
376 in isolation window)). (3) Average reporter signal/noise, representing the average tag
377 intensity for the PSM. (4) Presence of values within or below the notch, where the upper
378 boundary of the notch was used to identify PSMs with any values below this threshold.
379 The following values were used to filtering PSMs according to these metrics: (1) Delta
380 score > 0, 0.2 or 0.5, (2) Co-isolation < 100 %, 50 % or 10 %, (3) Average reporter S/N

381 > 0 or 10 (4) Notch PSMs retained or removed. All combinations of filtering thresholds
382 were performed, yielding 36 sets of filtered PSMs.
383
384 Aggregation to protein-level intensities involved removal of PSMs with missing values,
385 removal of proteins without at least two PSMs, and summation of PSM-level tag
386 intensities. Aggregation of PSM intensities to peptide-level intensities proceeded in the
387 same manner, but demanding at least two PSMs per peptide sequence.
388
389 *Statistical analysis*
390
391 To identify peptides and proteins with significant differential abundance, we used *limma*
392 [18] *Limma* was run with default settings, with the exception that we set trend=TRUE for
393 the eBayes function call, so that the prior variance was dependent on the trend between
394 feature intensity and observed variance. Protein intensity was modeled to depend on
395 condition, with results extracted for the contrast between 1x vs 2x and 1x vs 6x tags. P
396 values were adjusted for multiple testing within each PSM filtering schema, using the
397 Benjamini-Hochberg False Discovery Rate (FDR) procedure [19]. Features with FDR < 1
398 % were deemed to have significantly different intensity.
399
400 Yeast proteins with a significant increase in intensity and human proteins with a
401 significant decrease in intensity were deemed true positives (TP). Vis versa, significant
402 changes in the opposite direction were deemed false positives (FP). Proteins without
403 significant changes in intensity were deemed false negatives (FN).
404 F1 scores were calculated as the harmonic mean of recall (TP / (TP + FN)) and
405 precision (TP / (TP + FP)). No proteins were deemed true negatives (TN) since all
406 proteins should have a change in intensity.
407
408 *Extracting tune version from PRIDE submissions*
409 Dataset identifiers for 7072 studies using Orbitrap were obtained from ProteomeCentral
410 (http://proteomecentral.proteomexchange.org/cgi/GetDataset) by searching for entries
411 with 'Orbitrap' in the instrument text on 28 June 2021. These were further narrowed
412 down to 1525 studies in the PRIDE repository with 'Orbitrap Fusion', 'Orbitrap Fusion
413 Lumos' or 'Orbitrap Eclipse' listed as instrument since these share the same series of
414 signal acquisition software. Studies with multiple instruments listed were ignored to
415 avoid incorrectly asserting the version of Tune used. For each study, the smallest .raw
416 file was downloaded and the meta information extracted using the R package rawDiag
417 [20], including the version of the aquisition software, Tune. For 242 / 1525 studies, the
418 Tune version was not extracted either because the instrument detailed in the .raw file
419 was not one of the above Orbitraps, no .raw files were found, the downloaded .raw file
420 could not be parsed by rawDiag, or the .raw file URLs did not permit downloading.

421

Data availability

423

424 The mass spectrometry proteomics data have been deposited to the PRIDE Archive
425 (http://www.ebi.ac.uk/pride/archive/) via the PRIDE partner repository with the data set
426 identifier PXD027248.

427

428 All analyses and results are publically available from the github repo
429 https://github.com/CambridgeCentreForProteomics/notch, alongside the peptide
430 spectrum match (PSM)-level quantification from Proteome Discoverer, and reference
431 fasta databases used. Release v0.1 of the repository used for this manuscript is
432 archived with DOI 10.5281/zenodo.5105723.

433

Acknowledgements

435

440

Funding

448

Author Contributions

450

451 **TSS:** Conceptualization, Methodology, Formal analysis, Data Curation, Writing -
452 Original Draft, Writing - Review & Editing, Visualization, Project administration. **AA:**
453 Methodology, Investigation, Writing - Review & Editing. **JAC:** Methodology,
454 Investigation**,** Writing - Review & Editing. **OMC:** Methodology, Writing - Review &
455 Editing, Funding acquisition. **ME:** Formal analysis, Writing - Review & Editing, **KSL:**
456 Methodology, Writing - Review & Editing, Supervision, Funding acquisition.
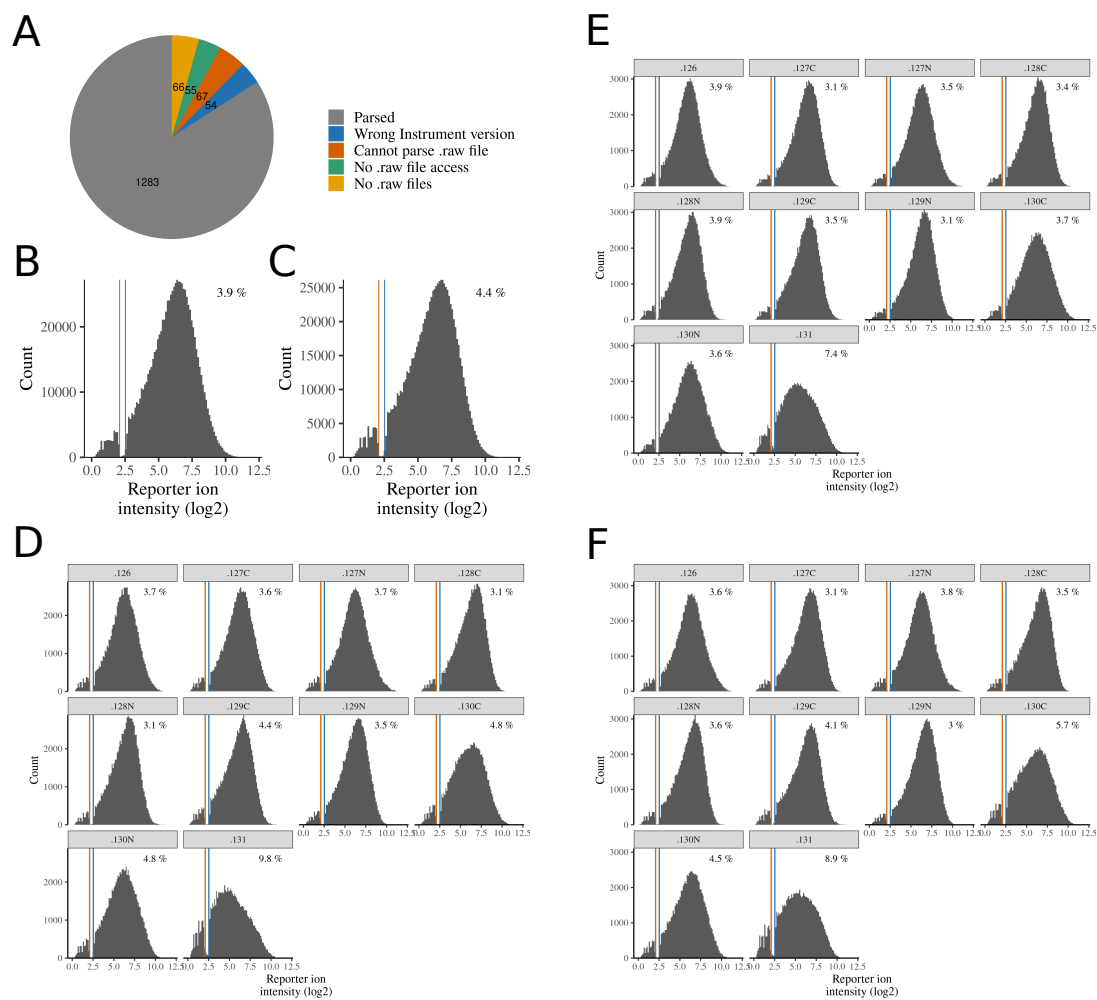
457

458 **Supplementary figures**

459
460 Figure S1.(A) The Tune version could be 'Parsed' from 1283 studies, with the remaining not accessible
461 for the reasons described. (B-C) The distribution of ion signals for TMT reporters for U-2 OS LOPIT-DC
462 replicate 2 (B) and replicate 3 (C). The approximate boundaries of the notch region are denoted by
463 vertical lines. The percentage of tag intensities below the upper boundary of the notch is stated in the top
464 right corner. (D-F) The distribution of ion signals for each individual TMT reporter; replicate 1 (D), replicate
465 2 (E) and replicate 3 (F).
466
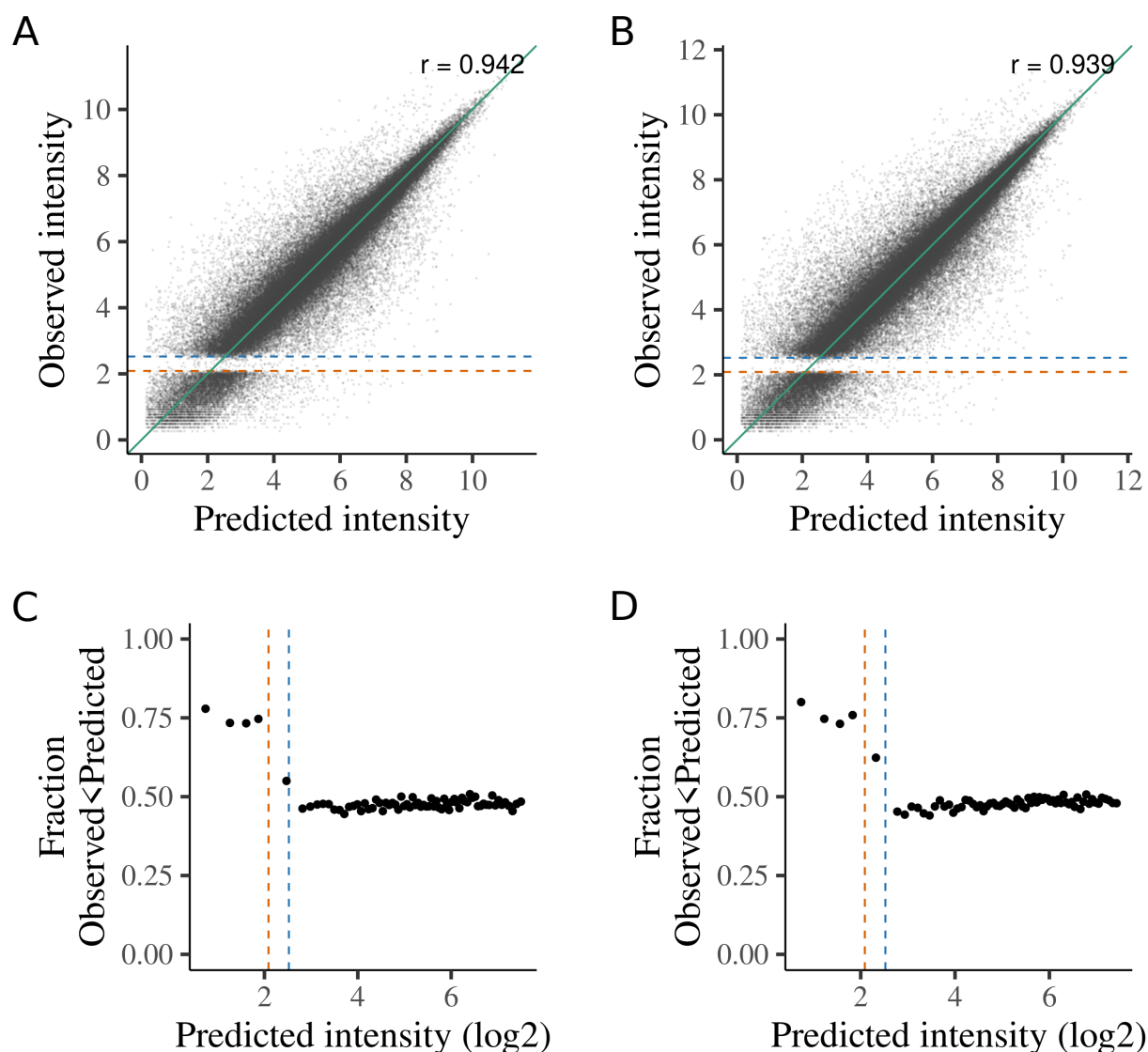
Figure S2: Characterisation of the reporter ion intensities around the notch in U-2 OS LOPIT-DC (A-B) Observed tag intensities vs predicted tag intensities for replicate 2 (A) and replicate 3 (B). Green line is equality. Pearson product-moment correlation coefficient shown in the top right corner. (C-D) Fraction of observed reporter ion intensities that are below the prediction for replicate 2 (C) and replicate 3 (D). Observed tag intensities below the notch are systematically underestimates relative to the prediction.
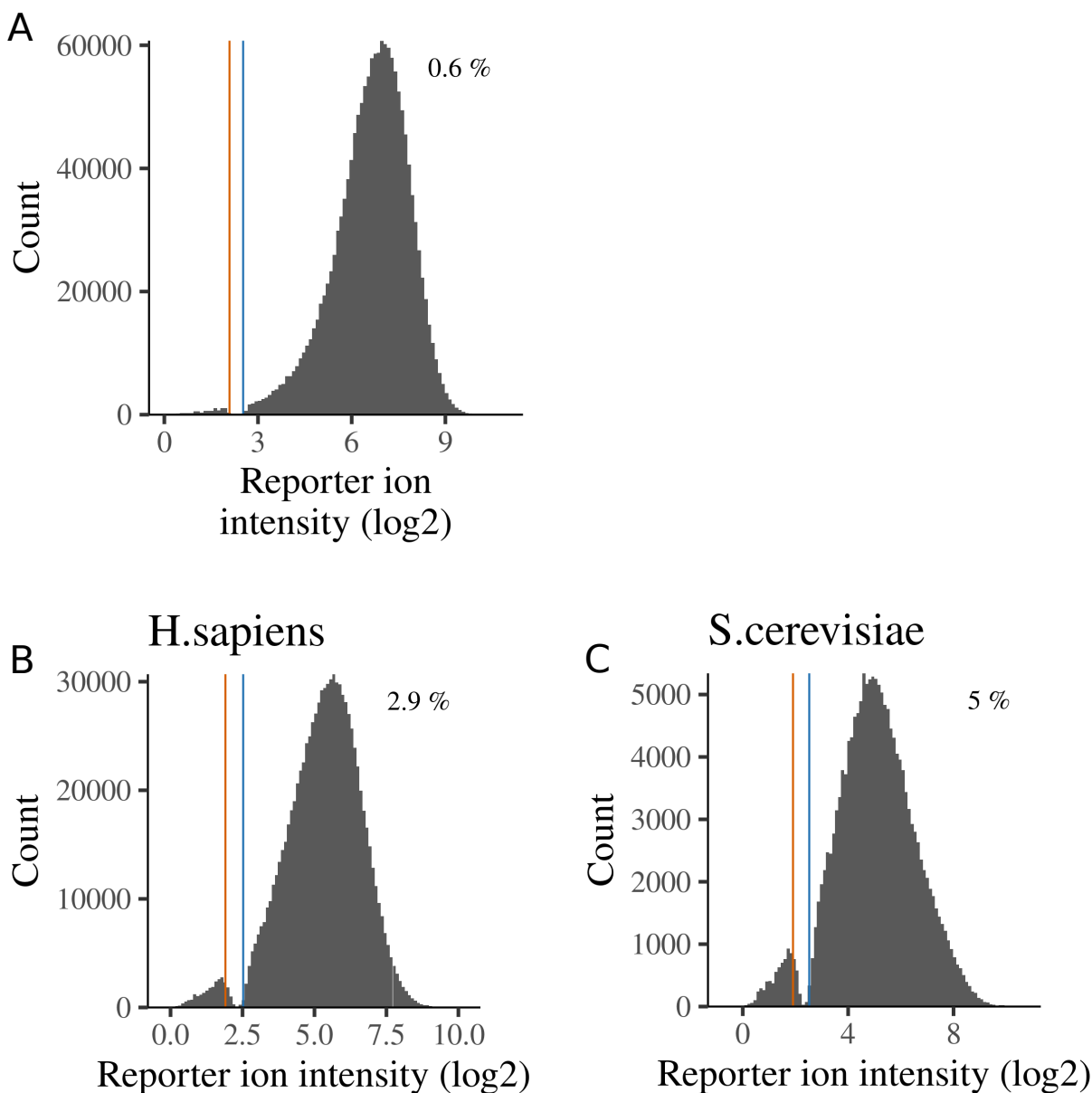
474
Figure S3. Distributions for reporter tag intensities in O'connell et al data (A; [4]) and the benchmark
dataset, considering only human (B) or yeast (C) proteins. The percentage of tag intensities below the
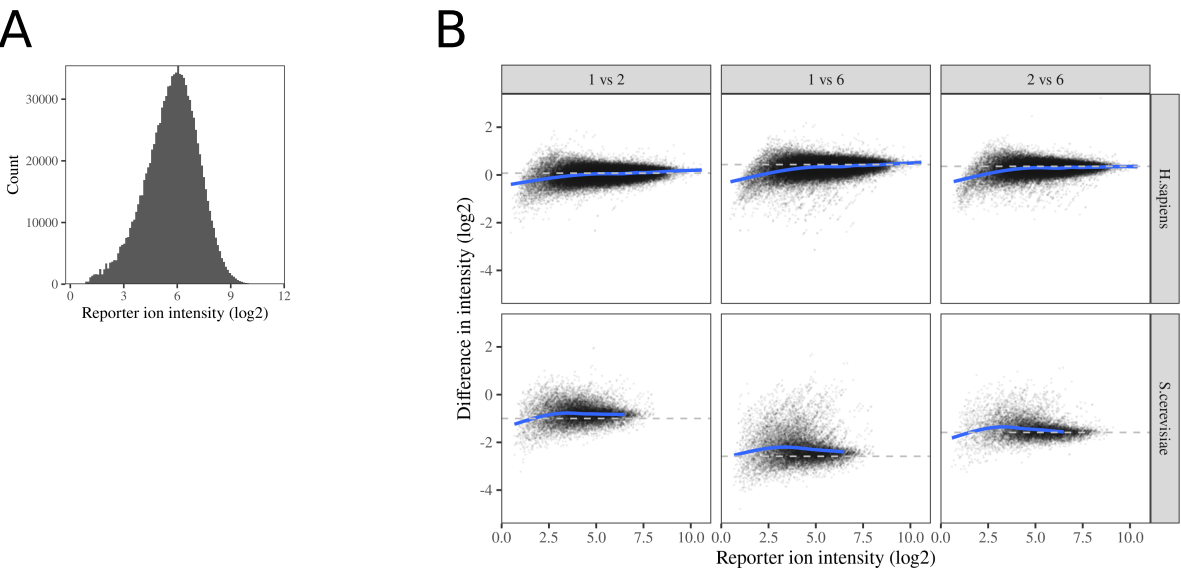upper boundary of the notch is stated in the top right corner.

479

480

481
482 Figure S4 Reporter ion intensity and fold-changes for benchmark dataset when using Tune 3.4.(A) The
483 distribution of reporter ion intensities for TMT reporters. No notch is observed. (B) The difference between
484 a single tag intensity and the mean tag intensity for a comparator group of tags. The ground truth is
485 denoted by a dashed horizontal line. The blue line presents a generalized additive smoothing model for
486 the relationship between tag intensity and intensity difference.
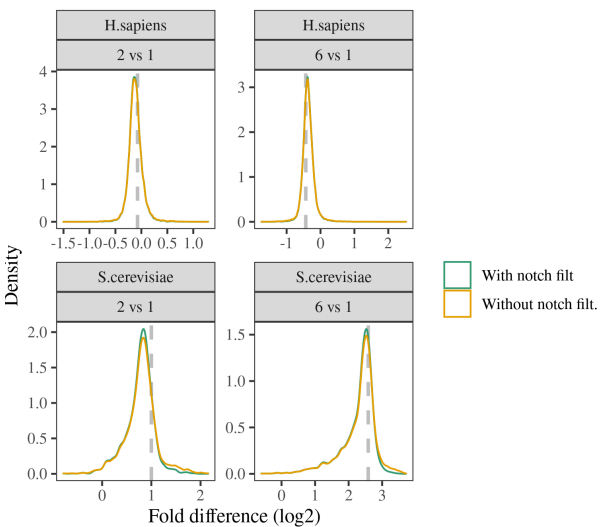
A
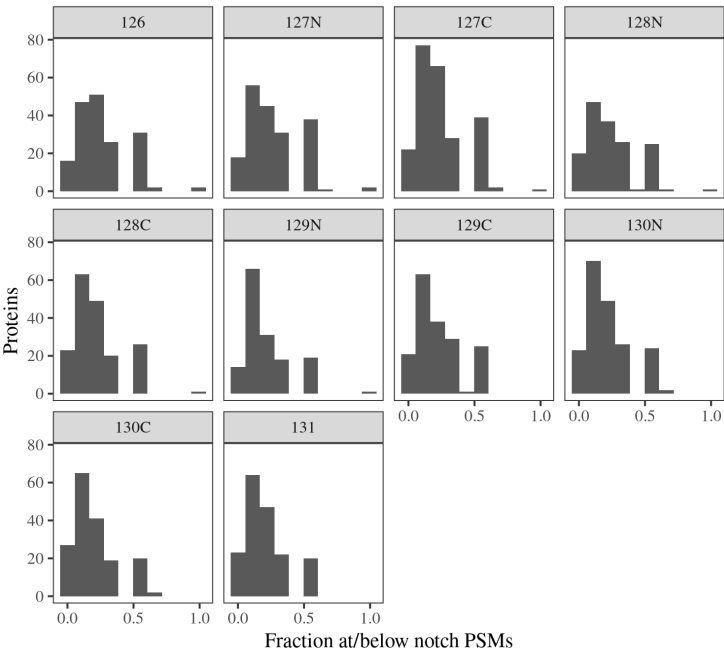
B
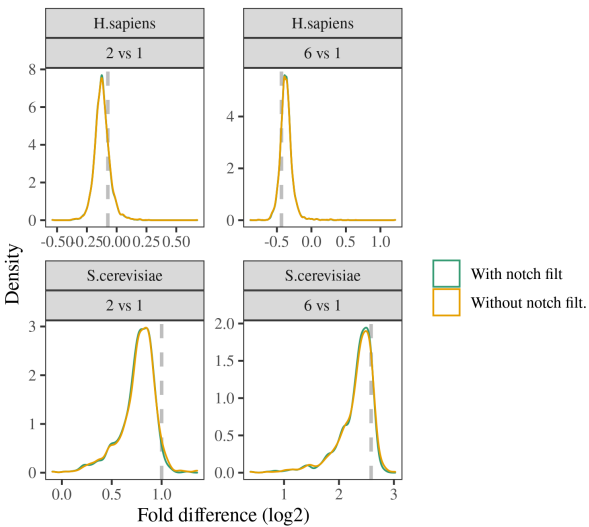
C

Figure S5. (A) Tallies for the fraction of the aggregated reporter ion intensities at or below the notch for each protein. Proteins with no intensities at or below notch are not tallied. (B-C) Observed fold-changes between tag groups, with and without notch filtering, for proteins (B) and peptides (C).
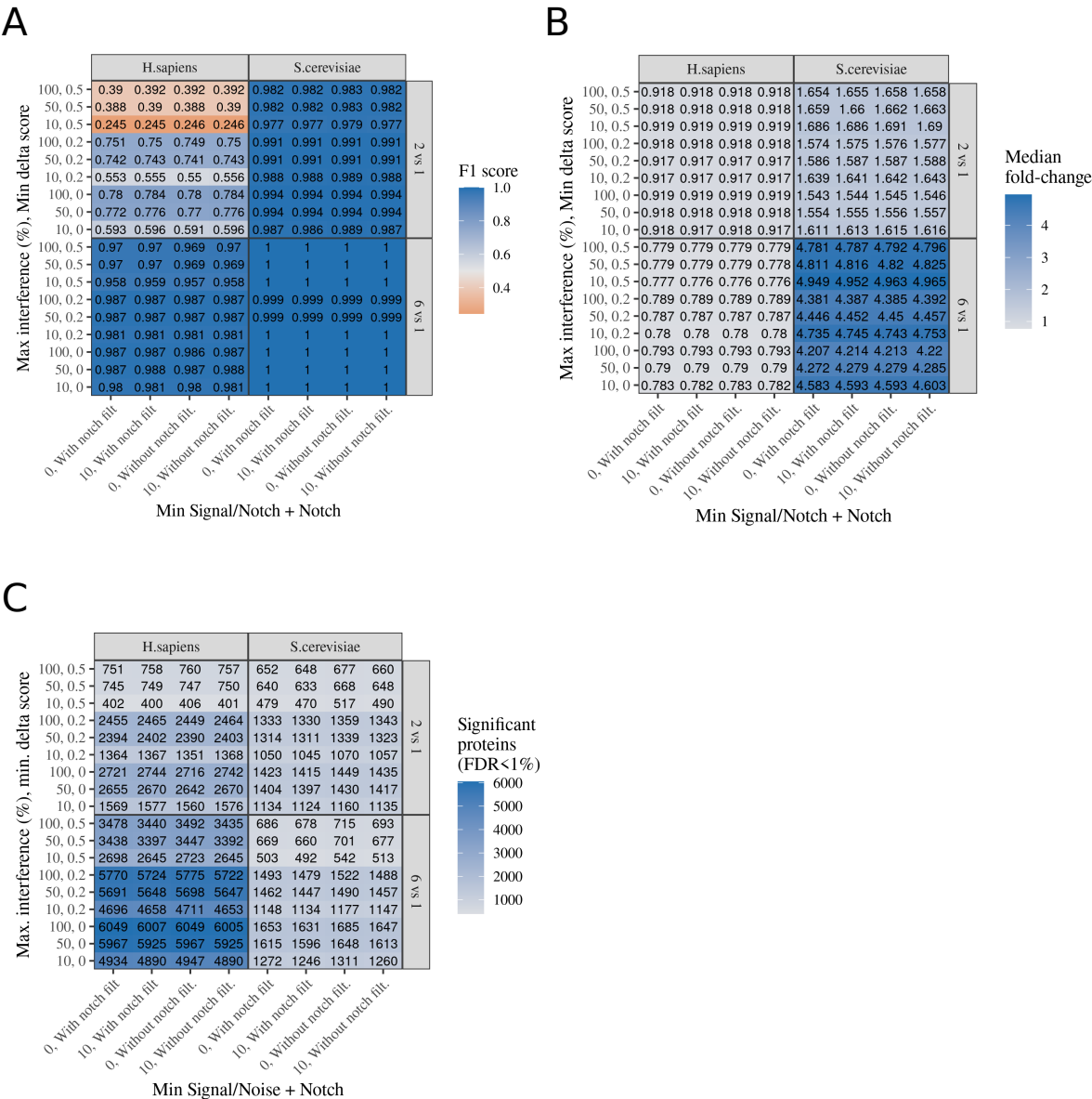
Figure S6. Summary of limma analysis of protein-level intensities. Limma analysis was performed on datasets generated from multiple different PSM filtering schemas, as indicated on the x-axis and y-axis. Each axes describe the combination of two filtering parameters. 'Min Signa/Noise' is the minimum average signal/noise for the PSM. '+ Notch' describes whether PSMs containing any intensities at or below the notch were removed. 'Max interference (%)' describes the maximum allowed interference/co-isolation. 'Min delta score' describes the minimum required delta score. (A) Accuracy of differential protein intensity detection, presented as the F1 score (harmonic mean of precision and recall). Only proteins present with all PSM filtering schemas were included (B) Median fold change between groups of tags. Only proteins present with all PSM filtering schemas were included. (C) The number of proteins with significantly different intensity.
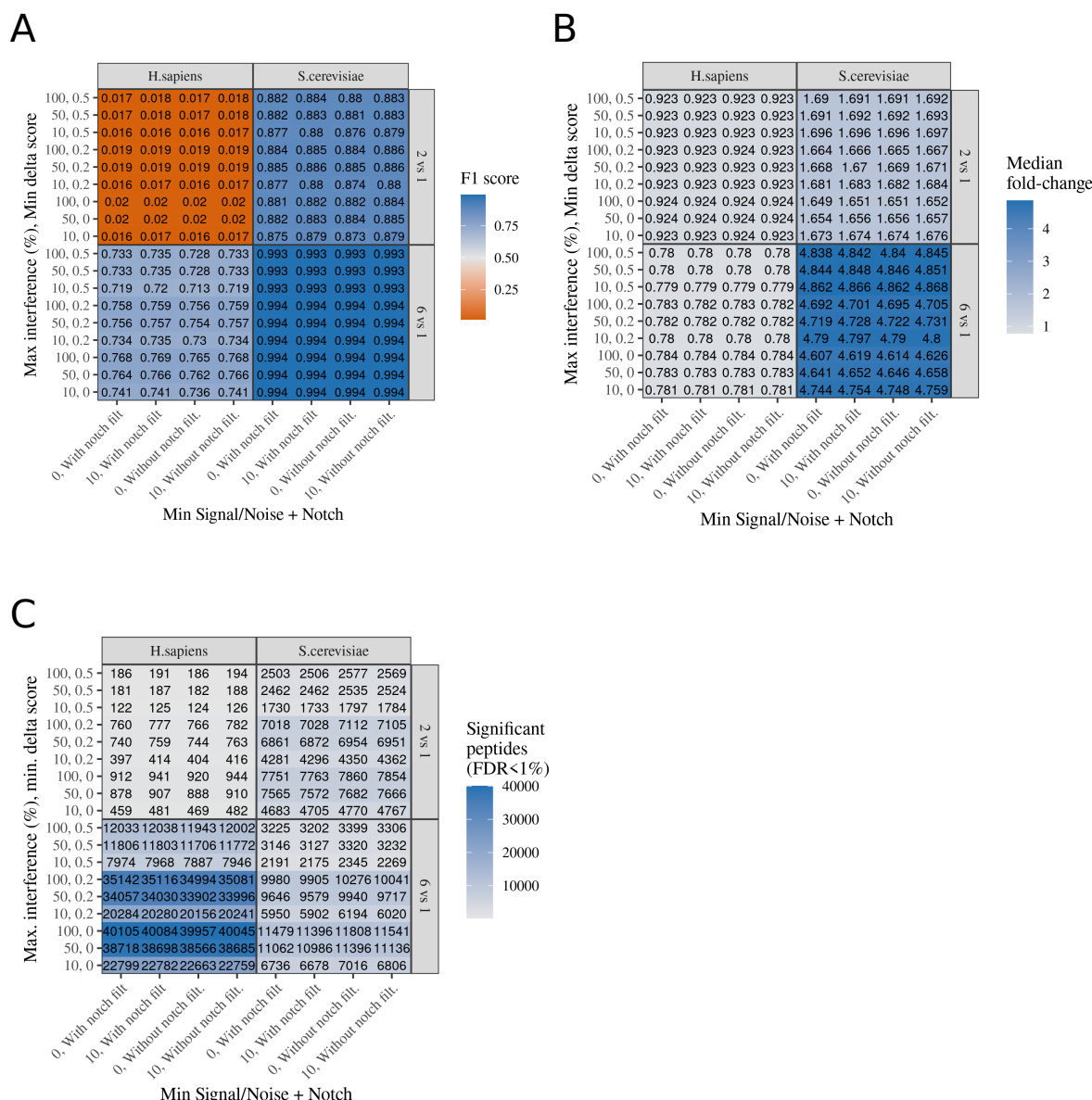
Figure S7. Summary of limma analysis of peptide-level intensities. Limma analysis was performed on datasets generated from multiple different PSM filtering schemas, as indicated on the x-axis and y-axis. Each axes describe the combination of two filtering parameters. 'Min Signa/Noise' is the minimum average signal/noise for the PSM. '+ Notch' describes whether PSMs containing any intensities at or below the notch were removed. 'Max interference (%)' describes the maximum allowed interference/co-isolation. 'Min delta score' describes the minimum required delta score. (A) Accuracy of differential protein intensity detection, presented as the F1 score (harmonic mean of precision and recall). Only peptide present with all PSM filtering schemas were included (B) Median fold change between groups of tags. Only peptide present with all PSM filtering schemas were included. (C) The number of peptides with significantly different intensity.

References

(1)   O'Brien, J. J.; Gunawardena, H. P.; Paulo, J. A.; Chen, X.; Ibrahim, J. G.; Gygi, S. P.; Qaqish, B. F. The Effects of Nonignorable Missing Data on Label-Free Mass Spectrometry Proteomics Experiments. *Ann Appl Stat* **2018**, *12* (4), 2075–2095. https://doi.org/10.1214/18-AOAS1144.

(2)   Bruderer, R.; Bernhardt, O. M.; Gandhi, T.; Miladinović, S. M.; Cheng, L.-Y.; Messner, S.; Ehrenberger, T.; Zanotelli, V.; Butscheid, Y.; Escher, C.; Vitek, O.; Rinner, O.; Reiter, L. Extending the Limits of Quantitative Proteome Profiling with Data-Independent Acquisition and Application to Acetaminophen-Treated Three-Dimensional Liver Microtissues. *Mol Cell Proteomics* **2015**, *14* (5), 1400–1410. https://doi.org/10.1074/mcp.M114.044305.

(3)   Rauniyar, N.; Yates, J. R. Isobaric Labeling-Based Relative Quantification in Shotgun Proteomics. *J Proteome Res* **2014**, *13* (12), 5293–5309. https://doi.org/10.1021/pr500880b.

(4)   O'Connell, J. D.; Paulo, J. A.; O'Brien, J. J.; Gygi, S. P. Proteome-Wide Evaluation of Two Common Protein Quantification Methods. *J Proteome Res* **2018**, *17* (5), 1934–1942. https://doi.org/10.1021/acs.jproteome.8b00016.

(5)   Pappireddi, N.; Martin, L.; Wühr, M. A Review on Quantitative Multiplexed Proteomics. *Chembiochem* **2019**, *20* (10), 1210–1224. https://doi.org/10.1002/cbic.201800650.

(6)   Li, J.; Cai, Z.; Bomgarden, R. D.; Pike, I.; Kuhn, K.; Rogers, J. C.; Roberts, T. M.; Gygi, S. P.; Paulo, J. A. TMTpro-18plex: The Expanded and Complete Set of TMTpro Reagents for Sample Multiplexing. *J. Proteome Res.* **2021**, *20* (5), 2964–2972. https://doi.org/10.1021/acs.jproteome.1c00168.

(7)   Hogrebe, A.; von Stechow, L.; Bekker-Jensen, D. B.; Weinert, B. T.; Kelstrup, C. D.; Olsen, J. V. Benchmarking Common Quantification Strategies for Large-Scale Phosphoproteomics. *Nat Commun* **2018**, *9* (1), 1045. https://doi.org/10.1038/s41467-018-03309-6.

(8)   McAlister, G. C.; Nusinow, D. P.; Jedrychowski, M. P.; Wühr, M.; Huttlin, E. L.; Erickson, B. K.; Rad, R.; Haas, W.; Gygi, S. P. MultiNotch MS3 Enables Accurate, Sensitive, and Multiplexed Detection of Differential Expression across Cancer Cell Line Proteomes. *Anal. Chem.* **2014**, *86* (14), 7150–7158. https://doi.org/10.1021/ac502040v.

(9)   Hughes, C. S.; Zhu, C.; Spicer, V.; Krokhin, O. V.; Morin, G. B. Evaluating the Characteristics of Reporter Ion Signal Acquired in the Orbitrap Analyzer for Isobaric Mass Tag Proteome Quantification Experiments. *J. Proteome Res.* **2017**, *16* (5), 1831–1838. https://doi.org/10.1021/acs.jproteome.7b00092.

(10)   *Orbitrap Fusion Series 3.0 Release Notes*; Thermo Fisher Scientific.

(11)   Geladaki, A.; Britovšek, N. K.; Breckels, L. M.; Smith, T. S.; Vennard, O. L.; Mulvey, C. M.; Crook, O. M.; Gatto, L.; Lilley, K. S. Combining LOPIT with Differential Ultracentrifugation for High-Resolution Spatial Proteomics. *Nature Communications* **2019**, *10* (1), 331. https://doi.org/10.1038/s41467-018-08191-w.

(12)   Navarrete-Perea, J.; Yu, Q.; Gygi, S. P.; Paulo, J. A. SL-TMT: A Streamlined Protocol for Quantitative (Phospho)Proteome Profiling Using TMT-SPS-MS3. *J Proteome Res* **2018**, *17* (6), 2226–2236. https://doi.org/10.1021/acs.jproteome.8b00217.

(13)   Fang, S.; Kirk, P. D.; Bantscheff, M.; Lilley, K. S.; Crook, O. A Bayesian Semi-Parametric Model for Thermal Proteome Profiling. *bioRxiv* **2020**, 2020.11.14.382747. https://doi.org/10.1101/2020.11.14.382747.

(14)   Mellacheruvu, D.; Wright, Z.; Couzens, A. L.; Lambert, J.-P.; St-Denis, N. A.; Li, T.; Miteva, Y. V.; Hauri, S.; Sardiu, M. E.; Low, T. Y.; Halim, V. A.; Bagshaw, R. D.; Hubner, N. C.; Al-Hakim, A.; Bouchard, A.; Faubert, D.; Fermin, D.; Dunham, W. H.; Goudreault, M.; Lin, Z.-Y.; Badillo, B. G.; Pawson, T.; Durocher, D.; Coulombe, B.; Aebersold, R.; Superti-Furga, G.; Colinge, J.; Heck, A. J. R.; Choi, H.; Gstaiger, M.; Mohammed, S.; Cristea, I. M.; Bennett, K. L.; Washburn, M. P.; Raught, B.; Ewing, R. M.; Gingras, A.-C.; Nesvizhskii, A. I. The CRAPome: A Contaminant Repository for Affinity Purification-Mass Spectrometry Data. *Nat Methods* **2013**, *10* (8), 730–736. https://doi.org/10.1038/nmeth.2557.

(15)   R Core team. *A Language and Environment for Statistical Computing.*; R Foundation for Statistical Computing: Vienna, Austria, 2020.

(16)   Wickham, H.; Averick, M.; Bryan, J.; Chang, W.; McGowan, L. D.; François, R.; Grolemund, G.; Hayes, A.; Henry, L.; Hester, J.; Kuhn, M.; Pedersen, T. L.; Miller, E.; Bache, S. M.; Müller, K.;

571   Ooms, J.; Robinson, D.; Seidel, D. P.; Spinu, V.; Takahashi, K.; Vaughan, D.; Wilke, C.; Woo, K.;
572   Yutani, H. Welcome to the Tidyverse. *Journal of Open Source Software* **2019**, *4* (43), 1686.
573   https://doi.org/10.21105/joss.01686.
574 (17) MSnbase, Efficient and Elegant R-Based Processing and Visualization of Raw Mass Spectrometry
575   Data | Journal of Proteome Research https://pubs.acs.org/doi/10.1021/acs.jproteome.0c00313
576   (accessed 2020 -11 -16).
577 (18) Ritchie, M. E.; Phipson, B.; Wu, D.; Hu, Y.; Law, C. W.; Shi, W.; Smyth, G. K. Limma Powers
578   Differential Expression Analyses for RNA-Sequencing and Microarray Studies. *Nucleic Acids Res.*
579   **2015**, *43* (7), e47. https://doi.org/10.1093/nar/gkv007.
580 (19) Benjamini, Y.; Hochberg, Y. Controlling the False Discovery Rate: A Practical and Powerful
581   Approach to Multiple Testing. *Journal of the Royal Statistical Society: Series B (Methodological)*
582   **1995**, *57* (1), 289–300. https://doi.org/10.1111/j.2517-6161.1995.tb02031.x.
583 (20) rawDiag: An R Package Supporting Rational LC–MS Method Optimization for Bottom-up
584   Proteomics | Journal of Proteome Research
585   https://pubs.acs.org/doi/10.1021/acs.jproteome.8b00173 (accessed 2021 -03 -09).
586